Applied Soft Computing 129 (2022) 109424

Contents lists available at ScienceDirect

Applied Soft Computing

journal homepage: www.elsevier.com/locate/asoc

Prediction of nonlinear structural response under wind loads using deep learning techniques

Smrithi Preetha Hareendran[1], Alice Alipour[2,*]

Department of Civil, Construction and Environmental Engineering, Iowa State University, Ames, IA, United States of America

ARTICLE INFO

Article history:
Received 31 January 2022
Received in revised form 19 July 2022
Accepted 25 July 2022
Available online 2 August 2022

Keywords:
Performance-based wind
Nonlinear response
Tall building
Deep learning techniques
LSTM

ABSTRACT

The wind actions on buildings are continuous in nature and could range from a few minutes to more than hours. Such long duration high intensity winds can push the structure to enter post elastic structural range and cause nonlinear behavior. Therefore, unlike performance-based earthquake engineering, where the structural simulations require seismic loads acting for a few seconds, the simulations for performance-based wind engineering (PBWE) requires wind load models acting for much longer durations. However, the nonlinear 3D model of a tall building will contain thousands of connections and structural members making it a complex finite element model. Dynamic time history analysis of such a model under loads lasting for hours can be tedious and often fail to achieve convergence. Using data-driven techniques that utilizes limited numerical and field data to obtain accurate structural responses under long duration loads is an exciting alternative. Deep learning techniques have been extensively used in the studies for structural health monitoring and earthquake engineering. However, the implementation of such data-driven techniques is very limited and has the potential for exploration in problems related to wind dynamics on tall buildings. This paper aims to predict the nonlinear structural response of tall buildings under sustained durations of wind loads using deep learning models. A Long Short-term Memory (LSTM) architecture is used to assess the efficiency of data-driven methods to replace computationally intensive 3D finite element analyses. The architecture will be tested on a 150 m tall building for response predictions under long duration wind loads. The robustness of the architecture will be further evaluated with predicting the acceleration response history of a scaled aeroelastic model based on experimental studies conducted at the Wind Simulation and Testing Laboratory (WiST) at Iowa State University.

1. Introduction

Understanding the structural response of tall buildings under dynamic loads such as seismic excitations and wind actions has gained much importance in the field of Performance-based design. Performance-based wind engineering (PBWE) is identified as the preferred design methodology for tall buildings subject to wind actions. This is because PBWE accounts for numerous sources of uncertainties involved in structural design. These include variations in wind loads arising from the unpredictable nature of wind velocities and turbulence intensities, the epistemic errors during measurement of data and the modeling of structure, in addition to the mechanical properties of the structure. Hence, the probabilistic PBWE framework has a higher potential of quantifying the structural reliability by acknowledging all of the uncertainties associated with a design problem.

The wind actions on buildings are nearly continuous and could last between a few minutes to multiple hours. Such long durations of high intensity winds can result in occupant discomfort, nonstructural damage and in some rare cases structural damage. Jafari and Alipour [1] present a detailed review of the wind induced vibrations experienced by tall buildings and Jafari and Alipour [2,3] and Abdelaziz et al. [4] presents methods of controlling excessive vibrations. To accurately characterize the performance of tall buildings under such loading combinations, the building models should capture the potential nonlinearity in structural response in addition to being able to simulate long durations of wind loads acting on the structure [5]. However, the nonlinear 3D model of a tall building will contain thousands of connections and structural members making it a complex finite element model. Dynamic time history analysis of such a model under loads lasting for hours can be tedious and often fail to achieve convergence. To address these aspects, this research

* Corresponding author.
E-mail address: alipour@iastate.edu (A. Alipour).
[1] PhD graduate, Department of Civil Construction and Envieronmental Engineering, Iowa State University
[2] Associate Professor, Department of Civil Construction and Envieronmental Engineering, Iowa State University

https://doi.org/10.1016/j.asoc.2022.109424
1568-4946/

aims to provide accurate structural responses by implementing data-driven techniques using limited numerical and field data.

In the past, significant amount of PBWE research focused on the structural behavior in the elastic or using simplistic models to capture the post-elastic response of structures. This was done to reduce the complexities arising from nonlinear modeling that requires computationally expensive simulations. Some such major studies towards addressing uncertainties in estimation of wind loads and development of the PBWE framework to assess damage, losses and occupant comfort were conducted by Micheli et al. [6–10], Ciampoli et al. [11,12] and Petrini et al. [13,14]. In 2019, ASCE published its first set of recommendations for PBWE in the form of Pre-standard for Performance-Based Wind Design [15] providing guidelines to implement PBWE in building designs to achieve an equal or superior performance objective compared to the prescriptive design methodology provided by ASCE 07-16 [16]. The guidelines provided include recommendations on the development of wind load model, analysis requirements and acceptance criteria for different performance objectives. The standard requires nonlinear time history analysis of buildings to satisfy the continuous occupancy performance objective and permits the use of such analyses in designing for occupant comfort and operational performance objectives as well. Hence, it can be concluded that PBWE requires analysis involving the complete wind load acting for longer durations such as 30 min, 1 h or a couple of hours. This is the primary reason for most of the PBWE research to adopt more simplistic models. Another approach to obtain accurate structural responses is implementing data driven techniques using limited numerical and field data.

Data driven techniques have been adopted by the engineering community for a couple of decades now. Several studies were conducted over the years highlighting the versatility of neural networks and deep learning. Studies by Pei et al. [17] and Smythe et al. [18] showed functions of layers, weights, biases, and activation functions in the neural networks to help model multilayer neural networks with the aim of implementing it in engineering problems such as prediction of nonlinear dynamics. Early implementations of machine learning (ML) techniques in time series forecasting were done on standard datasets, univariate and multivariate time series (Zhang et al. [19] and Xu et al. [20]). These studies focused on testing the effectiveness of ML models based on the number of nodes, hidden layers and training size of datasets. A number of studies adopted ML for seismic engineering purposes [18,21,22] to predict structural responses with studies conducted to forecast bridge responses. Several studies were also conducted in forecasting the seismic response of buildings [23,24].

Most of the adoptions of neural network models in wind design of buildings involved measurement of pressure coefficients and wind pressure distributions on building surfaces. Fu et al. [25] implemented Fuzzy neural networks for its ability to capture input–output relationships from limited amount of data to predict the wind pressure distributions and wind loads acting on large flat roofs. The predictions were accurate for varying wind directions and locations on roofs. The study concluded that such models could potentially lead to reduction in number of pressure sensors required in a model during wind tunnel tests. In another study Fu et al. [26] used Fuzzy Neural Networks to predict the mean and rms pressure coefficients, and time series of wind pressures on the roof of a large gymnasium. Comparisons were made with wind tunnel tests and Artificial Neural Networks (ANN) proved to be highly accurate in making predictions. Vyavahare and Nikose [27] used ANN for across wind response calculation based on static wind load calculations for buildings of varying aspect ratios and terrain conditions.

Nikose and Sanporote [28–31] implemented ANN for prediction of peak along-wind and across-wind responses in buildings. ANN was proposed to replace the quasi-static gust effect factor method given by Indian wind code to calculate the dynamic response of flexible tall buildings. ANN was shown to perform well in the predictions of shear force and bending moments in the along-wind direction at different heights of buildings. The study took into consideration the terrain categories and building aspect ratios. Dongmei et al. [32] determined the wind pressure coefficients and time series wind pressures acting on buildings using neural network architecture. The dataset was obtained from wind tunnel tests on a scaled high-rise building.

Bre et al. [33] developed an ANN-based analytical model to predict the mean wind pressure coefficients for every surface of low-rise buildings at every angle of attack (AOA). Validations were shown for different types of roof configurations. ANN proved to be more accurate than the parametric models whose performance was poor for varying building plan ratios and AOA's. Deep Neural networks (DNN) were used for prediction of wind pressure coefficients on low-rise gable roof buildings in the study by Tian et al. [34]. A scaled model was set up in the experimental facility and surface pressure coefficients were measured for different wind speeds, directions, and terrain features. This data was used in training and tested on winds acting from different directions not included in training. DNN provided accurate results, hence, reducing the number of potential experimental tests required to identify aerodynamic coefficients for unknown wind actions.

The nonlinear structural response forecasting using modified ANN's was explored by Lagaros and Papadrakakis (2012) [35] on buildings subjected to seismic loads. The study showed that adaptive ANNs were highly accurate in predicting nonlinear responses. Guarize et al. (2007) [36]was one of the first studies to use ANN to predict nonlinear structural responses under sustained durations of loading on mooring lines of marine structures. The training was done using short duration FEA (500 sec of loading) to predict responses up to 3 hr of loading. Wang and Wu [37] were the first to use deep learning to predict nonlinear structural response under wind loads. The study used physics-based governing equations and semi-empirical information to extract the loss functions to guide the training. However, the study only used simple SDOF system and MDOF system to present the architecture and failed to show applications in complex building systems. These studies establish that ANN's are capable of accurately predicting nonlinear structural behavior under long durations of loading.

To further the research on applicability of deep learning algorithms in wind engineering, this paper aims to predict the nonlinear structural response of tall buildings under sustained durations of wind loads using deep learning models. Here, the authors explore the efficiency of such data-driven techniques to replace computationally intensive 3-D finite element analyses. Long Short-Term Memory (LSTM) networks are a special category of neural networks, best suited for long time sequences as the network can capture long-term dependencies. Some studies that used LSTM models include Zhang et al. [38,39] where deep LSTM networks were used to predict nonlinear response for structures subjected to seismic loading and Peng et al. [40] used LSTM combined with fully convolutional networks to achieve higher performance in time series classification with minimum preprocessing of datasets. LSTM is also shown to outperform several other deep learning methods in the case of autoregression of time-series estimations and is highly robust and insensitive to noise in training data. Hence, in this paper, the authors develop an LSTM architecture capable of capturing structural behavior under sustained durations of wind loading.

The architecture will be tested on a 150 m tall building for response predictions under long duration wind loads. Structural information for the development of analytical model and calculation of gravity and wind loads for the nonlinear dynamic time

history analyses are explained in the forthcoming sections. The training of LSTM architecture is done based on the finite element analysis data on the given tall building for the design wind speed of 130 mph for 9 min of loading. Testing is performed on the next 21 min of loading thus having a testing to training ratio of 70/30 (%). The aim is to explore if a well-conditioned LSTM model can make accurate predictions of nonlinear structural response with limited numerical data for training. The robustness of the architecture will be further evaluated with predicting the acceleration response history of a scaled aeroelastic model based on experimental studies conducted at the Wind Simulation and Testing Laboratory (WiST) at Iowa State University.

2. Deep learning and LSTM architecture

Neural networks were developed in the 1940s as a subset of machine learning to emulate the biological signaling of neurons in human brain. Neural networks consist of hidden layers of nodes each acting as a linear regression function to extract natural features from the input and map them to the output.
With the advancement in computational technology and availability of vast amounts of data for training, design of deep learning neural networks are possible today. In a traditional neural network, the information only moves in one direction between input and output. These networks have no memory of the past except what it learned in training and hence has no notion of time. Recurrent neural networks (RNN) are a class of deep learning neural networks that are capable of modeling sequential data. Long Short-Term Memory (LSTM) networks are a special category of RNN, best suited for long time sequences as the network can capture long-term dependencies. Hence, LSTM has gained popularity in the field of data-driven response prediction over the past few years.

2.1. LSTM cell architecture

An LSTM network has a recursive loop in its cell that retains memory for long durations. Fig. 1 shows the LSTM architecture used in the study and highlights a hidden layer in the LSTM cell architecture. From the figure it can be seen that the LSTM cell contains four neural network layers interacting with each other. The most important component in an LSTM cell is the cell state or the memory cell at time t, $c^{\langle t\rangle}$ which holds the necessary characteristic information and transfers it to the next time step. The inputs to the LSTM cell at any time t are $c^{\langle t-1\rangle}$, $a^{\langle t-1\rangle}$ and $x^{\langle t\rangle}$ where $a^{\langle t-1\rangle}$ is the output activation function from the previous time step and $x^{\langle t\rangle}$ is the input vector of the current time step. The input gate calculates $\tilde{c}^{\langle t\rangle}$ using a *tanh* function which is a candidate for updating memory cell in the current time step.

Eq. (1) shows the calculation of $\tilde{c}^{\langle t\rangle}$ where b_c is the bias function. The decision to update is made using the update gate which has a sigmoid activation function that keeps the values at either 0 or 1, Eq. (2).

$$\tilde{c}^{\langle t\rangle} = tanh\left(w_c\left[a^{\langle t-1\rangle}, x^{\langle t-1\rangle}\right] + b_c\right) \tag{1}$$

$$\Gamma_u = \sigma\left(w_u\left[a^{\langle t-1\rangle}, x^{\langle t\rangle}\right] + b_u\right) \tag{2}$$

The forget gate in the architecture is used to selectively remove the least relevant information from the output of the previous time step. The gate also uses a sigmoid activation function, Eq. (3). The forget gate also removes the vanishing gradient issues during backpropagation typical in RNNs.

$$\Gamma_f = \sigma\left(w_f\left[a^{\langle t-1\rangle}, x^{\langle t\rangle}\right] + b_f\right) \tag{3}$$

The current cell state is determined from the outputs of forget gate and input gate as given by Eq. (4).

$$c^{\langle t\rangle} = \Gamma_u \times \tilde{c}^{\langle t\rangle} + \Gamma_f \times c^{\langle t-1\rangle} \tag{4}$$

Finally, the output activation function of the current time step is calculated with the output gate using sigmoid functions.

$$\Gamma_o = \sigma\left(w_o\left[a^{\langle t-1\rangle}, x^{\langle t\rangle}\right] + b_o\right) \tag{5}$$

$$a^{\langle t\rangle} = \Gamma_o tanh \times c^{\langle t\rangle} \tag{6}$$

From the given equations it can be seen that all of the gate values are calculated using $a^{\langle t-1\rangle}$ and $x^{\langle t\rangle}$. So, as long as the forget and update gates are set appropriately, it is straightforward for LSTM cell state $c^{\langle t\rangle}$ to be passed along the memory over a long time. It should also be noted that in a series architecture, all the variables including $a^{\langle t\rangle}$, $a^{\langle t-1\rangle}$, $x^{\langle t\rangle}$, $x^{\langle t-1\rangle}$, weight functions and biases are matrices and vectors. Therefore, it is important to understand that all the multiplication operations shown in the equations are elementwise.

2.2. Data processing

The structural response parameters chosen for the study are the displacements and accelerations as these responses are adopted as the primary quantification metric to characterize structural/non-structural damage in all the international codes and design standards. The time sequence of displacement response for the 44-story building is obtained from the dynamic nonlinear time-history analysis performed using OpenSees at a wind speed of 130 mph.

The aerodynamic forces acting on any tall building consist of the stochastic forces due to fluctuating winds known as buffeting loads and the aeroelastic flutter instability due to self-excited forces resulting from the interaction of the structure with wind. The equations of motion for wind-induced response of a tall building at any height, z, and time, t is given by Eqs. (7)–(9) [41].

$$\text{Across wind response: } m(\ddot{h}(z,t) + 2\varsigma_h\omega_h\dot{h}(z,t) + \omega_h^2 h(z,t)) = L_B(z,t) + L_{se}(z,t) \tag{7}$$

$$\text{Along wind response: } m(\ddot{p}(z,t) + 2\varsigma_p\omega_p\dot{p}(z,t) + \omega_p^2 p(z,t)) = D_B(z,t) + D_{se}(z,t) \tag{8}$$

$$\text{Torsional response: } I\left(\ddot{\alpha}(z,t) + 2\varsigma_\alpha\omega_\alpha\dot{\alpha}(z,t) + \omega_\alpha^2\alpha(z,t)\right) = M_B(z,t) + M_{se}(z,t) \tag{9}$$

In the above equations, m is the mass per unit height (H) of the building, I is the mass moment of inertia about the centroidal axis per unit height (H), [ς_h, ω_h], [ς_p, ω_p] and [ς_α, ω_α] are the critical damping ratio and natural frequency in the across-wind, along-wind and torsional modes of vibration, [$\ddot{h}$, $\dot{h}$, h], [$\ddot{p}$, $\dot{p}$, p] and [$\ddot{\alpha}$, $\dot{\alpha}$, α] are the acceleration, velocity and displacement in the across-wind, along-wind and torsional directions respectively. $L_B(z, t)$, $D_B(z, t)$, and $M_B(z, t)$, represent the buffeting loads per unit height (H) in across-wind, along-wind and torsional directions and $L_{se}(z, t)$, $D_{se}(z, t)$ and $M_{se}(z, t)$ represent the self-excited loads per unit height in across-wind, along-wind and torsional directions acting on the structure. The effects of self-excited loads were incorporated into the datasets used by substituting the mechanical damping (C_{mech}) of the building models with effective damping (C_{eff}) that includes the combined effects of both mechanical and aeroelastic damping in terms of flutter derivatives. The effects of aeroelastic stiffness on the overall stiffness of the building were neglected because these are usually negligible. The wind loads, displacement and acceleration responses at every floor level were recorded (Hareendran et al. [42]) Further details on the analyses and structural responses are discussed in the study presented.

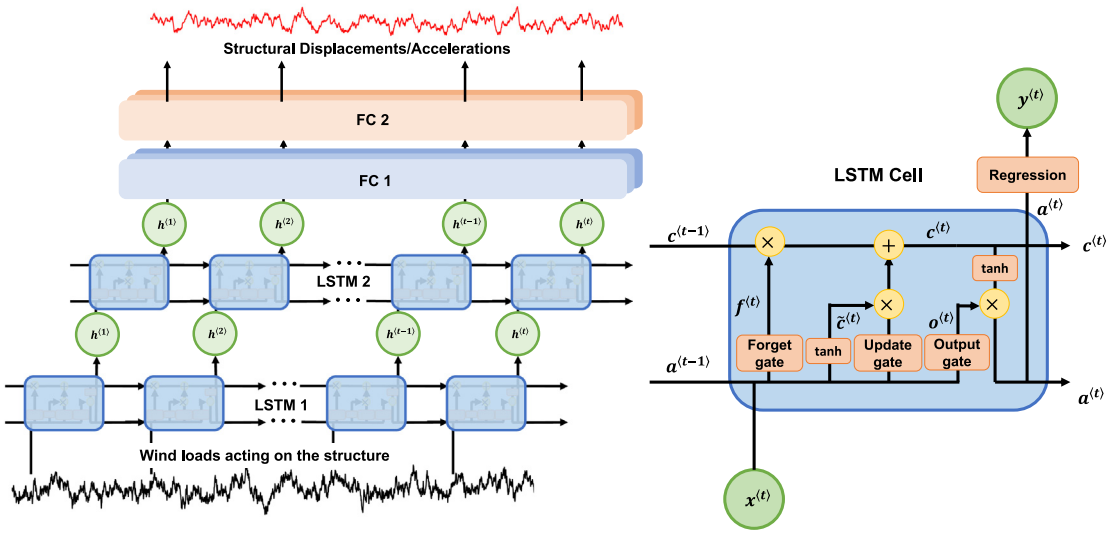

(a) (b)

Fig. 1. (a) LSTM network architecture used in the study with the wind loads as the input layer, first LSTM layer (LSTM 1) with 100 neurons, second LSTM layer (LSTM 2) with 100 neurons and two fully connected layers FC 1 and FC 2 with 100 neurons each and the structural displacements/accelerations as the output layer, (b) individual LSTM cell with its components.

2.3. LSTM network architecture

To evaluate the performance of LSTM model, the time history data of input and output features are split into training, validation, and testing sets. In this study, the aim is to predict long duration responses (30 min or more) given the structural responses under a much shorter duration (9 min) of loading. Hence, training/testing and training/validation are selected as 30/70 and 90/10 respectively. Two steps of data preprocessing were involved in this study. First was the data scaling which is critical for faster convergence of LSTM model as it uses *tanh* and sigmoid functions that are sensitive to the scale of input data. The MinMaxScaler preprocessing class with limits of [-1 1] is used to scale the data. The training and validation datasets were scaled using the MinMaxScaler within the specified range to provide the most accurate predictions. The second was the split sequencing of the data. Split sequencing refers to the stacking of time series data with a time lag. In this study the long time series data is converted into multiple data samples with reduced dimensions of time steps and each sample has an overlap of a few seconds data with the previous sample. This is a modification to the stacked model used by Zhang et al. [39] where it was recommended that an LSTM with stacked sequencing of data performs better than a full sequence of time series data and also reduces the computational cost. Fig. 2 shows the split sequencing of data used in the study.

A typical LSTM architecture consists of multiple LSTM layers in combination with fully connected (*FC*) or dense layers and often dropout layers in addition to the input and output layers. The complete LSTM model is also shown in Fig. 1. The model consists of two hidden LSTM layers with 100 blocks or neurons each. A dropout layer is added in between the LSTM layer and *FC* layer to randomly drop neurons during training. The loss is estimated using mean square error. Adam is the optimization algorithm used to train the network as it has been proven to be more computationally efficient compared to other optimization algorithms available. The parameters for adam include learning rate (alpha) and decay rates of moving averages (beta1 and beta2). The default parameters used by tensorflow ($\alpha = 0.001, \beta_1 = 0.9, \beta_2 = 0.999$) are used in the LSTM model. A linear activation function is used in the output layer of the LSTM model here as typical to regression models.

3. Decision variables and validations using analytical building models

The decision variables (*DV*) in PBWE are chosen to assess the performance of structures. The *DV*s chosen in this study are the structural displacements and floor accelerations as they are universally accepted as the parameters to quantify building responses and resulting damage. The international standards such as International Building Code (*IBC)* (2018) [43], *AISC-360* (2016) [44], *ACI-318* (2019) [45] etc. use displacements to identify the propagation of structural and non-structural damage and the accelerations are used to evaluate the human perception of motion or occupant comfort in the building. The displacement and acceleration responses will be predicted based on the analytical results and an experimental study.

The building used for the validations have the benchmark Commonwealth Advisory Aeronautical Council (CAARC) configuration with a height of 528 ft. (∼160 m). The steel beams in the frames have a span of 26.25 ft. (8 m) with 6 spans along the longer direction and 4 spans in the perpendicular direction. The 3D view of the building is shown in Fig. 3. The building frames are composed of rectangular cross sections built-up from wide flanged I-sections for the columns and wide flanged I-sections for the beams. The building was designed under static loads based on the provisions of AISC 360 (2016) and ASCE 7 (2016) for a design wind speed of 130 mph for Miami Dade county in Florida. The static analysis, and design was conducted in SAP2000 [46] and frame sections were chosen to satisfy the structural and serviceability requirements.

To conduct the nonlinear time-history analysis of the whole time–history of the wind events, the structure was modeled in OpenSees [47]. OpenSEES is a software framework for developing applications to simulate the performance of structural

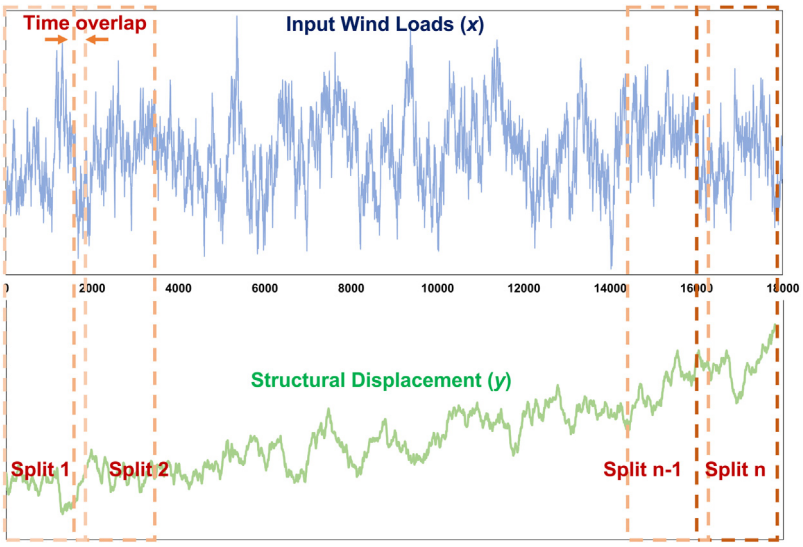

Fig. 2. Split sequencing of data.

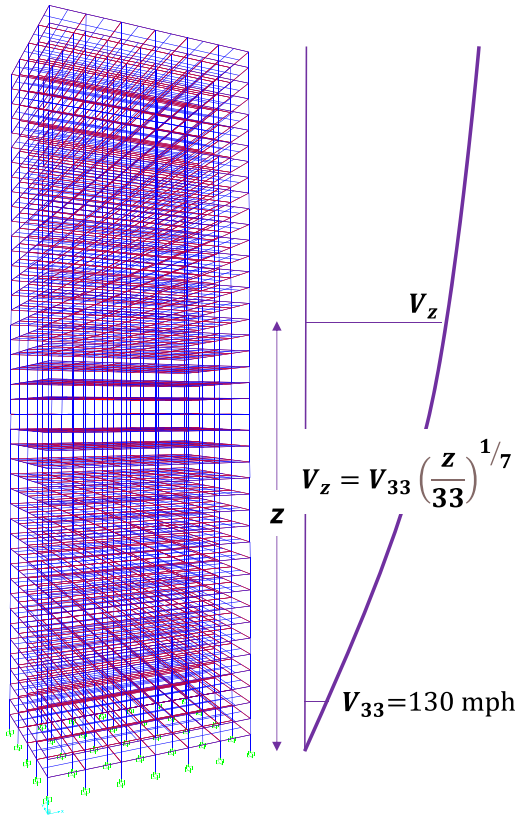

Fig. 3. Analytical model of the 44-story building along with the wind speed profile.

and geotechnical systems subjected to earthquakes. Hence, the software is also capable of performing nonlinear time-history analysis under wind loads. The member sections were modeled using the fiber section function inbuilt in the OpenSees library. This enabled modeling each section as a group of fibers with a specific uniaxial material, area and location. The number of fibers along the width and thickness dimensions were taken as 6 and 1, respectively. The materials and elements available in the OpenSees library were used in the development of the model. The nodes were assigned based on the respective story heights and frame spacing. The beam–column elements were modeled using force-based element available in OpenSees library. Force-based elements were based on distributed plasticity models that allow for spread of plasticity along the element. These elements allow yielding to occur anywhere along the element.

The nodes in each floor are assigned to a diaphragm using the rigid diaphragm function. The beams and columns of the frame are composed entirely of structural steel members. The material from the OpenSees library, Steel02 (Giuffre-Menegotto-Pinto Model) was used to model the members which has a yield stress, $F_y = 50$ ksi (345 MPa) and modulus of elasticity, $E = 29\,000$ ksi (2×10^5 MPa) with isotropic hardening properties. The parameters used in the material definition to transition from elastic region to post yield behavior includes a strain hardening ratio of 0.05, $R_0 = 15$, $c_{R1} = 0.925$, and $c_{R2} = 0.15$. The structural damping was set to 2 percent and Rayleigh damping was used.

The mass of the structural components was defined in terms of mass density and was assigned with the element definitions. The additional loads acting on the structures included the superimposed dead loads and live loads along with the wind forces. The dead and live loads considered in the design were chosen from ASCE-07 (2016) conforming to the requirements of an office building. The dead and live loads were applied on the model as uniformly distributed floor loads. The wind loads consisting of turbulent buffeting forces were applied to the nodes on the surface along and across the direction of wind flow. The design wind speed of Miami-Dade County (130 mph based on ASCE 07-16) and an exposure category C was used in the structural analysis. The wind loads were applied at zero-degree angle of incidence. The directionality of wind has not been explicitly explored in the study because the building is designed without the knowledge of orientation of worst wind. The directionality factor of K_d given by ASCE 07-16 was taken as 1.0 in the calculation of wind loads during the design of building. Hence, there is no reduction of wind loads based on directionality of wind which leads to a more conservative design.

The training data for LSTM was obtained based the nonlinear dynamic time-history analyses conducted on the building. The analysis was conducted for 30-minute duration loads for the design wind speed of 130 mph. The turbulent wind loads were applied in the along-wind, across-wind and torsional directions. The building was analyzed for gravity and wind actions using nonlinear dynamic time history analysis. The time step of loading

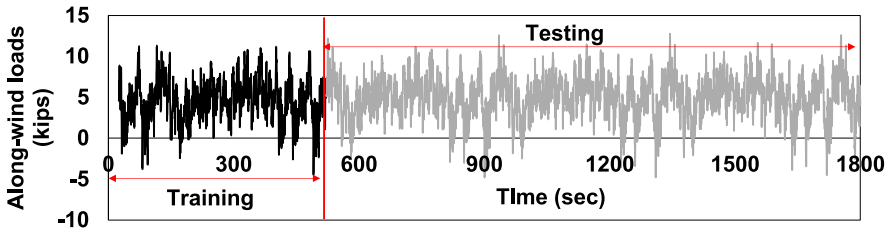

Fig. 4. Splitting of the training and testing datasets with the example of an along-wind loading. Training data is 30% and the testing data is 70%.

was 0.1 s, and the building displacements and accelerations were recorded at every floor level. The results from the time history analysis were observed to show much higher responses at the beginning of the analyses because of the sudden loads acting on the structure. Those results were filtered out when analyzing and reporting the time-history responses used in the study. The training data for the LSTM network consisted of turbulent wind loads in the along-wind, across-wind and torsional directions as input features and floor displacements and accelerations as the output required for predictions. The wind loads, floor displacements and accelerations for every level along the height of the building was chosen for training and testing. Fig. 4 shows the along wind loads acting at a specific height on the building for the duration of 30 min highlighting the training and testing datasets.

4. Results and discussion

The LSTM network architecture is evaluated by forecasting the time-history of the nonlinear response of a 44 steel MRF building model. The training data consists of 44 datasets containing time-histories of wind loads and structural displacements each with a length of 1800 s (18 000-time steps). The 130-mph wind speed is the reference wind speed or 3-s gusts acting at 33 ft (10 m) height from the base of the building. The wind speed profile varies over the height of the building based on the power law formulations given as $V_z = V_{33}\left(\frac{z}{33}\right)^{1/7}$ where, V_z is the wind speed at any height z along the building and V_{33} is the 3-s gust acting at 33 ft above the ground. The wind loads are applied at every floor level of the building.

The data is split into training, testing and validation datasets. A validation set is different from a test set as it is a part of the training data itself. The validation data is used to identify the points of overfitting in the algorithm as well as to determine the accuracy of the algorithm. With the 4 input features being the timestep and wind loads in the along and across-wind and torsional directions, the input training dataset has a size of [5325 × 4], validation dataset has the size of [533 × 4] and testing dataset has a size of [12,425 × 4]. The corresponding output datasets have sizes of [5,325 × 1], [533 × 1] and [12,425 × 1] for the training, validation and testing, respectively. Each stack has a chosen width of 5 time steps which was determined as the optimum stack size based on an iterative analyses with stack widths varying between 1 and 20. Therefore, the size of each input sample dataset was [5 × 3,550] and output dataset sample was [5 × 3,550]. The network was also subjected to an iterative analysis to determine the number of epochs which resulted in the lowest validation error. Overfitting was observed to occur for analyses with over 35 epochs.

The displacement forecasting using LSTM network in the along-wind and across-wind directions are shown in Figs. 5 and 6, respectively. The predictions were made for every floor level, however, only 4 levels (14, 24, 34 and 44 stories) are shown in the figures for concise presentation. LSTM forecasting in the along-wind and across-wind directions for accelerations are given by Figs. 7 and 8, respectively.

From Figs. 5 and 6 it can be seen that LSTM architecture was able to capture the displacement responses in both directions with high accuracy. The network was capable of capturing the peaks and gradients in the response efficiently. The figures also show the true errors at each time step and as well as the 90th percentile bounds. The errors are much lower than 10% in both directions with a few outliers with higher errors. Fig. 9(a) shows the LSTM performance in capturing the maximum displacements in the along-wind and across-wind directions. It can be said that although not accurate, the peak displacement predictions are reasonable with a low margin of error (less than 0.1 m). Based on Figs. 7 and 8, it can be said that the acceleration predictions are not as accurate as that of displacements. This can be seen from the errors reported in the figures. This could be on account of higher variations between time steps where it was more gradual for displacement responses. The model is still able to capture the peak accelerations with a small margin of error as shown in Fig. 9(b). This margin of error could be acceptable when considering LSTM as a powerful tool capable of potentially replacing the computationally expensive analytical methods.

The correlation coefficients for the response predictions in two lateral directions are shown in Fig. 10. The coefficients calculate the correlation between LSTM predictions and analytical models at all floor levels for the given time-history. Fig. 10(a) shows very high correlation coefficients (>0.98) for displacements in along-wind and across-wind directions. This shows that LSTM predictions are very close to the analytical model predictions. Although, not significantly lower, for the purpose of reading the figure, the 31st story is highlighted showing the lowest correlation coefficients in both the directions for displacements. The correlation coefficients for accelerations in both directions are compared in Fig. 10(b). The figure shows higher correlations in the across-wind direction than along-wind predictions. The coefficients are lower than that of displacements. The figure shows values greater than 0.90 for most of the floor levels with 2nd floor having the lowest values and highlighted in the figure. Hence, from the figure, it can be said that the acceleration predictions were also reasonably accurate.

The hysteretic responses in the along-wind and across-wind directions were compared with LSTM models and are presented in Fig. 11(a) and (b). The comparisons were made to understand if the LSTM was capable of capturing the outlying responses from the analytical model results. The figures presented here show that LSTM is indeed capable of capturing such behavior and is able to do so for along-wind and across-wind responses. This again shows that LSTM is highly capable of retaining memory and capturing time-dependent and path-dependent (non-elastic/plastic) behaviors of the building components.

5. Validation using experimental time history analysis data

The LSTM network architecture was tested using the data from an experimental study on the aeroelastic model of the CAARC building configuration. The experimental studies were conducted at the Aerodynamic and Atmospheric Boundary Layer

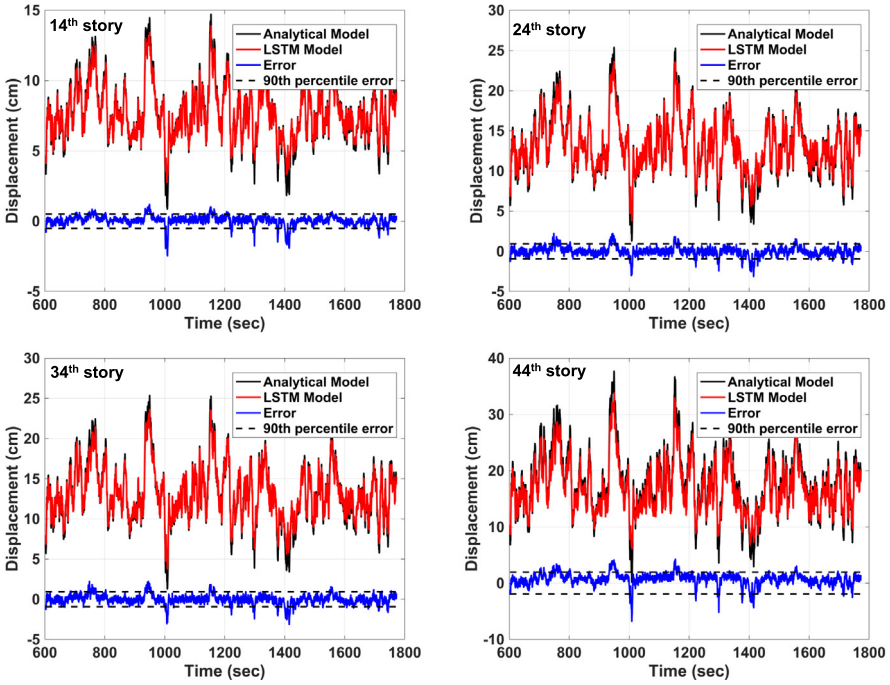

Fig. 5. LSTM performance in along-wind displacement predictions with a testing/ training ratio of 70/30 along the height of the building at 14th, 24th, 34th and 44th story.

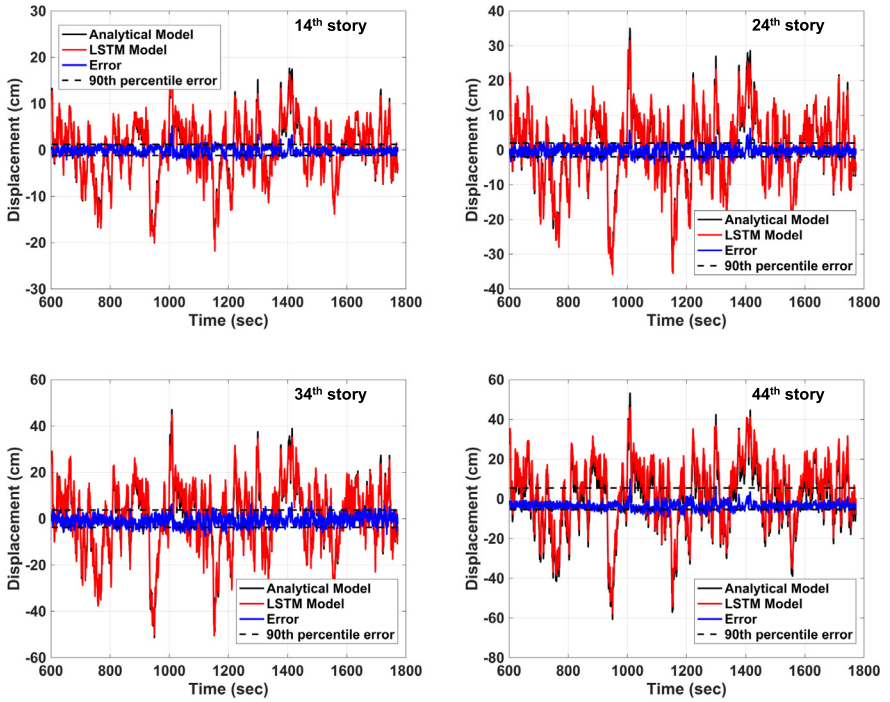

Fig. 6. LSTM performance in across-wind displacement predictions with a testing/ training ratio of 70/30 along the height of the building at 14th, 24th, 34th and 44th story.

(AABL) Wind Simulation and Testing Laboratory, Iowa State University [48]. The full-scale building was 600 ft. (182.9 m) tall with aspect ratios of $B/D = 1.5$ and $H/D = 6.0$. The aeroelastic model used for the testing had reduced dimensions calculated for a geometric scale ratio of 1/175. The full-scale and model dimensions of the building are given in Table 1.

The model was tested in boundary-layer wind generated in the ABL test section, which had a cross section of 8.0 ft. (2.44 m) width $\times$ 7.25 ft. (2.21 m) height with a maximum mean wind speed of 89.3 mph (40 m/s). Four triangular spires were mounted at equal spacing at the beginning of the wind tunnel test section and wooden blocks with different size and spacing were distributed on the wind tunnel floor in front of the aeroelastic model to simulate a boundary layer flow. The layout of wooden blocks was arranged to simulate a suburban terrain. The damping ratios of the model were measured as 0.69%, 0.62% and 0.24% in the -x, -y and α directions respectively.

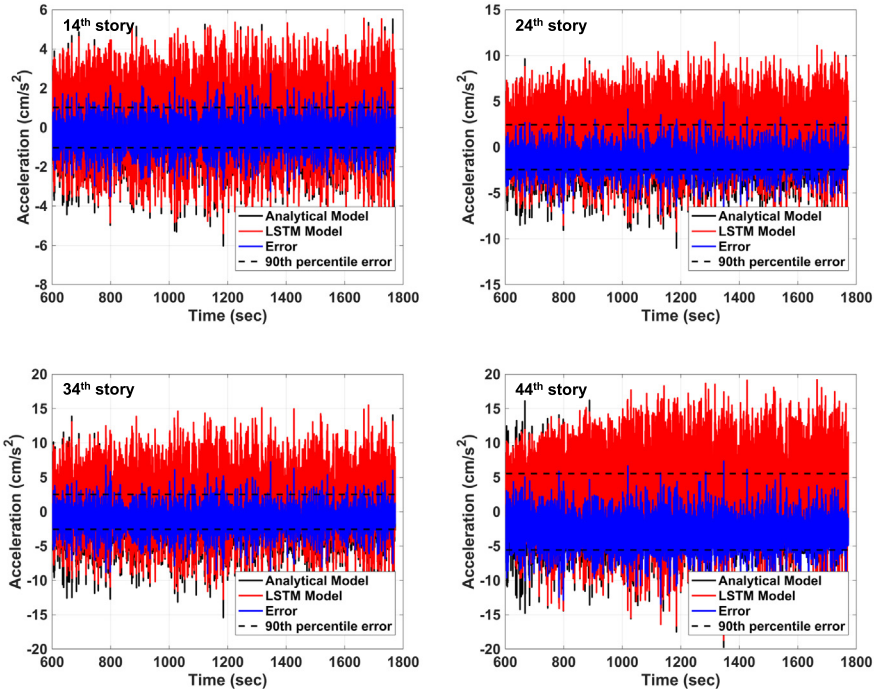

Fig. 7. LSTM performance in along-wind acceleration predictions with a testing/ training ratio of 70/30 along the height of the building at 14th, 24th, 34th and 44th story.

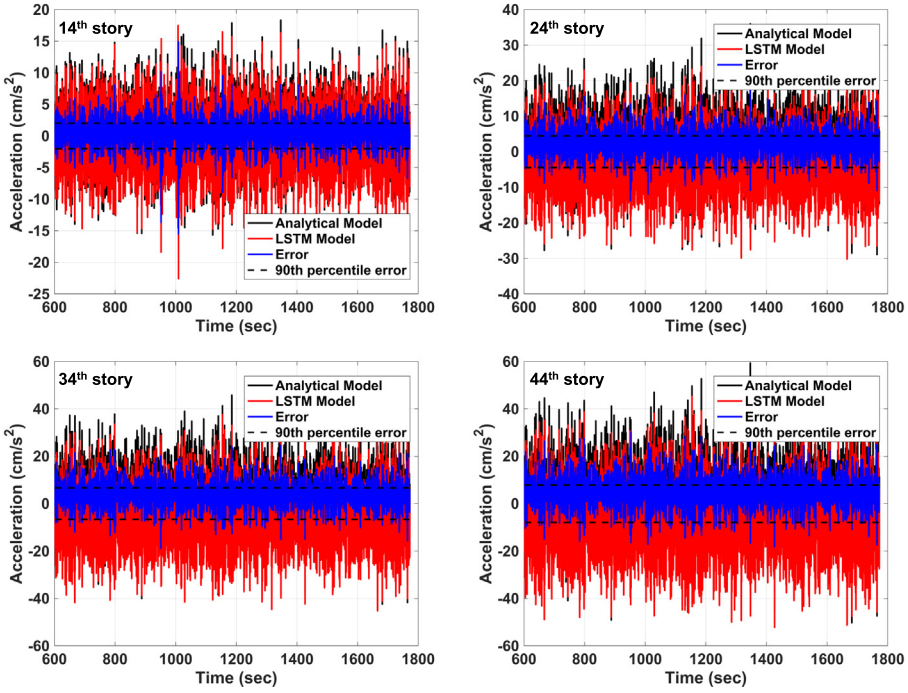

Fig. 8. LSTM performance in across-wind acceleration predictions with a testing/ training ratio of 70/30 along the height of the building at 14th, 24th, 34th and 44th story.

Table 1
Properties of the full-scale and aeroelastic models of the CAARC building.

	Height, H (m)	Depth, D (m)	Width, B (m)	Natural frequency (Hz)		
				Lateral (-x)	Lateral (-y)	Torsional (α)
Full-scale building	182.9	30.5	45.7	2.5	2.5	3.0
Aeroelastic model	1.05	0.17	0.26	0.2	0.2	

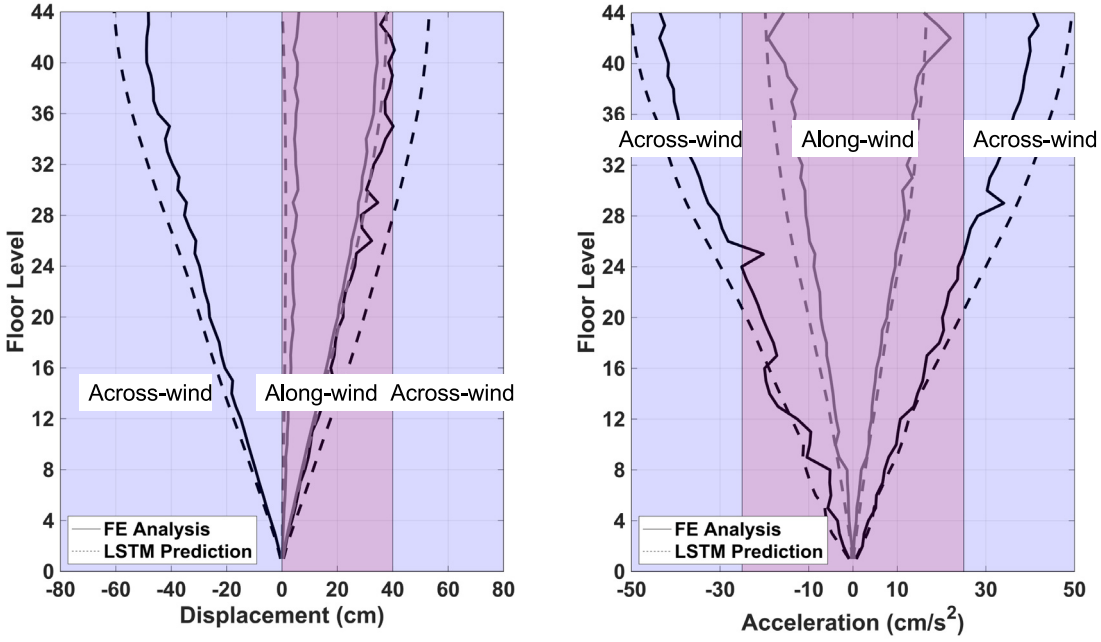

Fig. 9. LSTM performance in maximum response predictions along the height of building (a) displacements and (b) Accelerations.

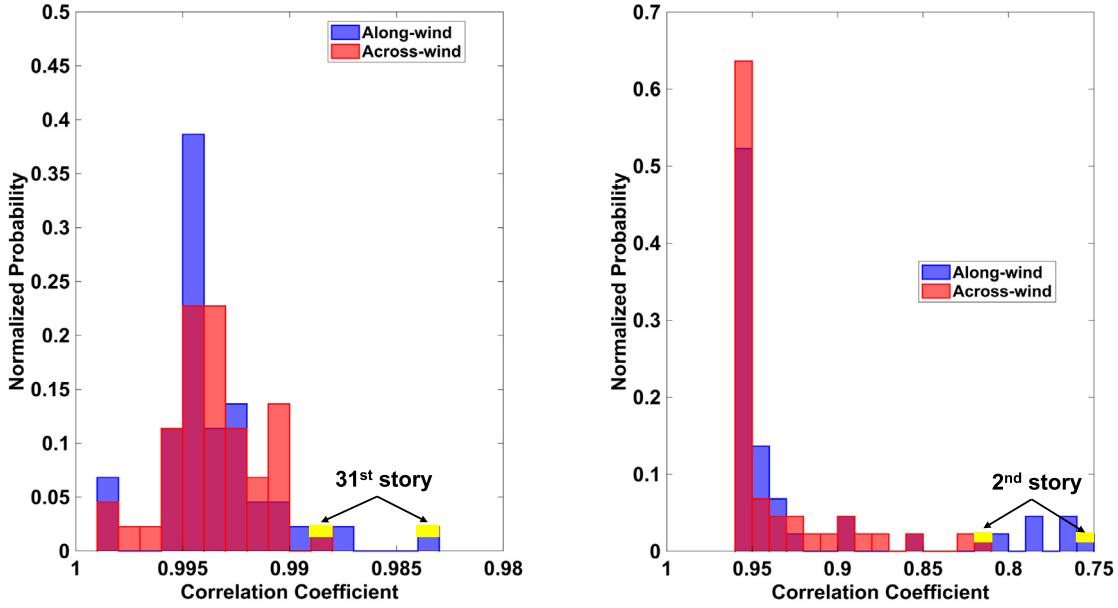

Fig. 10. Correlation coefficients showing prediction performance for (a) displacements and (b) accelerations.

The wind profile of the approaching boundary layer flow was measured at different elevations in front of the model through which mean wind speed and turbulence intensity were acquired with a sampling frequency of 312.5 Hz and a time period of 60 s (690 s in full-scale). The measurements of wind-induced vibration of aeroelastic tall building model were achieved by six uni-directional accelerometers (PCB Model 352C65), which were attached to the panels of the model at two different levels, namely, roof-height (H) and mid-height (0.55H). The locations of the accelerometers as well as the definition of angle of attack (AOA) and building coordinates (x, y and α) are illustrated in Fig. 12. The acceleration data was recorded with a sampling frequency of 100 Hz for a duration of 60 s (690 s in full-scale). The model was tested under different wind speeds, represented by U_H, which is the wind speed at roof height of the model, and three wind directions.

To characterize the incoming flow for the ABL tests, wind speed measurements were carried out along the centerline of the

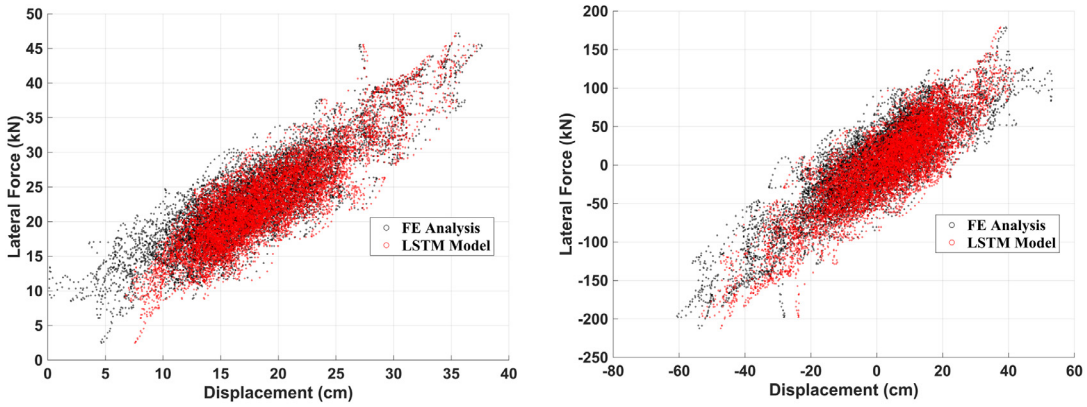

Fig. 11. Comparison of restoring force–displacement curves in the (a) along-wind and (b) across-wind directions based on LSTM and analytical model results.

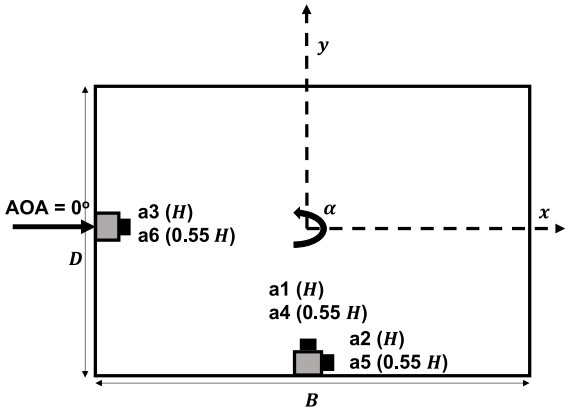

Fig. 12. Illustration of the building model with the coordinate system, angle of attack (AOA) and locations of accelerometers.

wind tunnel with vertical heights ranging from 3 in. (76.2 mm) to 45 in. (1143 mm). During the measurement of the mean wind-speed profile, the mean wind speed (U_H) at the building roof height (Z_H) was kept constant as 11.65 mph (5.21 m/s). The measured mean wind speed was curve-fitted with a power-law function. The exponent of the fitted power-law function was estimated as 0.34, which matched very well with the value representing the high-suburban or low-urban terrain suggested by Architectural Institute of Japan, where most tall buildings are located. In addition to the mean wind speed, the turbulence intensities of the ABL wind in u (longitudinal), v (lateral) and w (vertical) directions were calculated using the definition $I_{ii} = \frac{\sigma_{ii}(z)}{U(z)}$, where $i = u$, v or w, $\sigma_{ii}(z)$ is the root mean square of the velocity fluctuations and $U(z)$ is the mean wind speed at the corresponding height (z). The turbulence intensity at roof height Z_H were $I_{uu} = 17.7\%$, $I_{vv} = 13.5\%$ and $I_{ww} = 11.3\%$, respectively. Time histories of wind-induced vibration at zero-degree angle of attack (AOA $= 0°$) in x, y and α directions were measured by the accelerometers at the roof height of the building model (H).

The training data for the acceleration response prediction of the aeroelastic model consisted of 6 datasets containing time stamp and acceleration responses along three directions of motion. Each dataset contains 6000-time steps corresponding to 60 s of wind loading at a sampling rate of 100 Hz. Here the problem is that of a univariate time series forecasting where the output from the previous time step is used as the input to the next time step for making predictions. In this case each time step was walked one at a time, and the predicted test acceleration was made available to forecast the acceleration at the next time step. This is also known as the persistence forecast where the prediction at time step t-1 is used to make prediction at time step t. The stack width in this study is 1. The datasets each with 6000-time steps was split into training/validation and training/testing data in the ratio of 0.9/0.1 and 0.8/0.2 respectively. The validation error was observed to be minimum at 40 epochs.

Fig. 13 shows the acceleration response predictions obtained from LSTM. It can be seen that the predictions are very accurate from Fig. 13(a) and (b). The figures also show that LSTM is able to capture the maximum responses accurately for a univariate time series data in the absence of additional input characterizing the structural properties.

6. Fragility curves and loss functions

Fragility analysis is a standardized methodology employed in the performance-based structural design against wind and seismic hazards. The objective of a fragility analysis is the computation of conditional probability of exceedance of damage measures such as inter story drift ratios, peak accelerations etc. corresponding to a specific feature of dynamic response. FEMA has developed methods to correlate the response of the buildings under seismic hazards to the structural and non-structural damage and its ramifications in terms of the downtime or repair costs set by the stakeholders. From the extensive database, three structural and non-structural components are chosen in this study to illustrate the process. These are welded column splices, cold-formed steel walls and gypsum partition walls given in Table 2. The progress and characterization of various damage states in each of the structural/non-structural components is given in column 4 of Table 2.

The procedure used in the development of fragility curves is shown in Fig. 14. The probability of exceedance corresponding to each damage state may be used to evaluate the losses due to repair or replacement of the component. The cost of repair/replacement for the fragility groups are also given by FEMA and can be obtained from the FEMA P-58 database.

In this study, the loss ratio is the parameter used, which is the ratio of repair to replacement cost. So, if the loss ratio is reported as 1, it means the cost of repair is either equal to or greater than the cost of replacement and that the component must be replaced. The probability of exceedance corresponding to the highest story drift ratio is obtained from the fragility curves. The study compares the losses computed based on analytical models to those from LSTM predictions. For this reason, the fragility

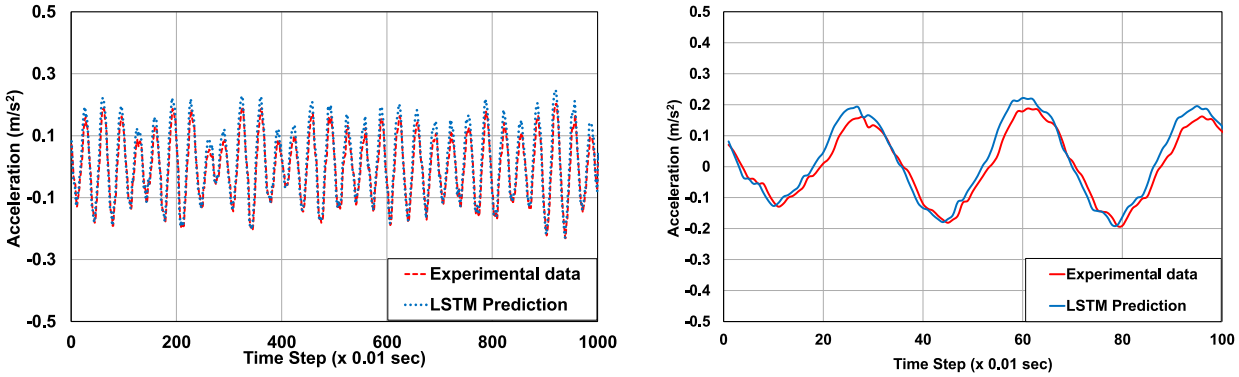

Fig. 13. LSTM Prediction of the structural response under an unknown turbulent wind action on the aeroelastic building model (a) The acceleration response of the test set along *x*-direction (b) zoomed in to show the acceleration response for the first 100 time steps.

Table 2
Properties of the full-scale and aeroelastic models of the CAARC Building.

Structural/Non-structural components	Damage parameter	Damage states	Description	Median/Dispersion
Welded column splices	Story drift ratio	DS1/DS2, DS3	**DS1**: Ductile fracture of the groove weld flange splice. Damage in field is either obscured or deemed to not warrant repair. No repair conducted.	0.02/0.4
			DS2: Ductile fracture of the groove weld flange splice	0.02/ 0.4
			DS3: DS1 followed by complete failure of the web splice plate and dislocation of the two column segments on either side of the splice.	0.05/ 0.4
Cold formed steel walls	Story drift ratio	DS1, DS2	**DS1**: Pull out of sheathing fasteners from studs.	0.019/ 0.3
			DS2: Buckling of steel sheathing. Buckling of framing members.	0.019/ 0.25
			DS2: Glass falls from frame.	0.0107/ 0.35
Gypsum wall partitions	Story drift ratio	DS1, DS2, DS3	**DS1**: Screw pop-out, cracking of wall board, warping or cracking of tape, slight crushing of wall panel at corners.	0.004/ 0.45
			DS2: Moderate cracking or crushing of gypsum wall boards (typically in corners). Moderate corner gap openings, bending of boundary studs.	0.011/ 0.35
			DS3: Buckling of studs and tearing of tracks. Tearing or bending of top track, tearing at corners with transverse walls, large gap openings and walls displaced.	0.019/ 0.25

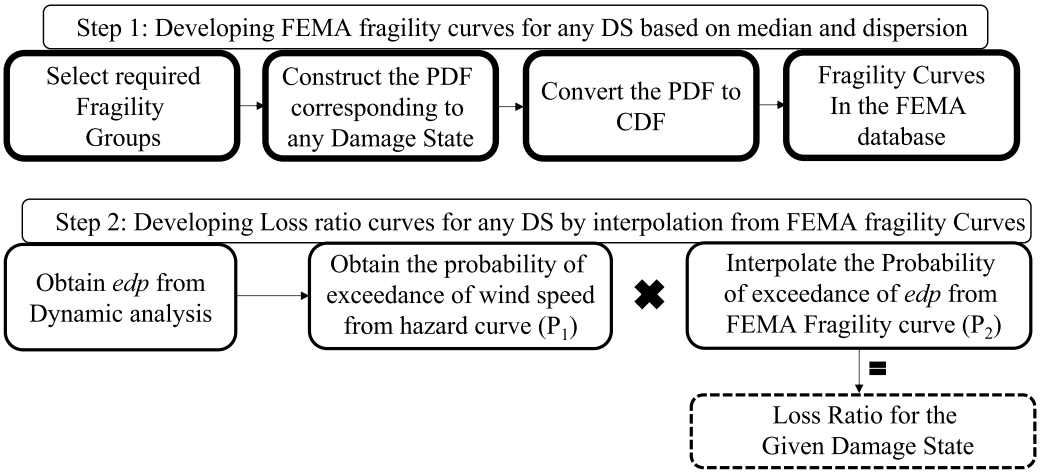

Fig. 14. Graphical representation of the development of fragility curves for calculation of losses to structural/non-structural components.

curves are not shown here as the focus is on illustrating the capability of LSTM to predict the loss ratios and not on the process

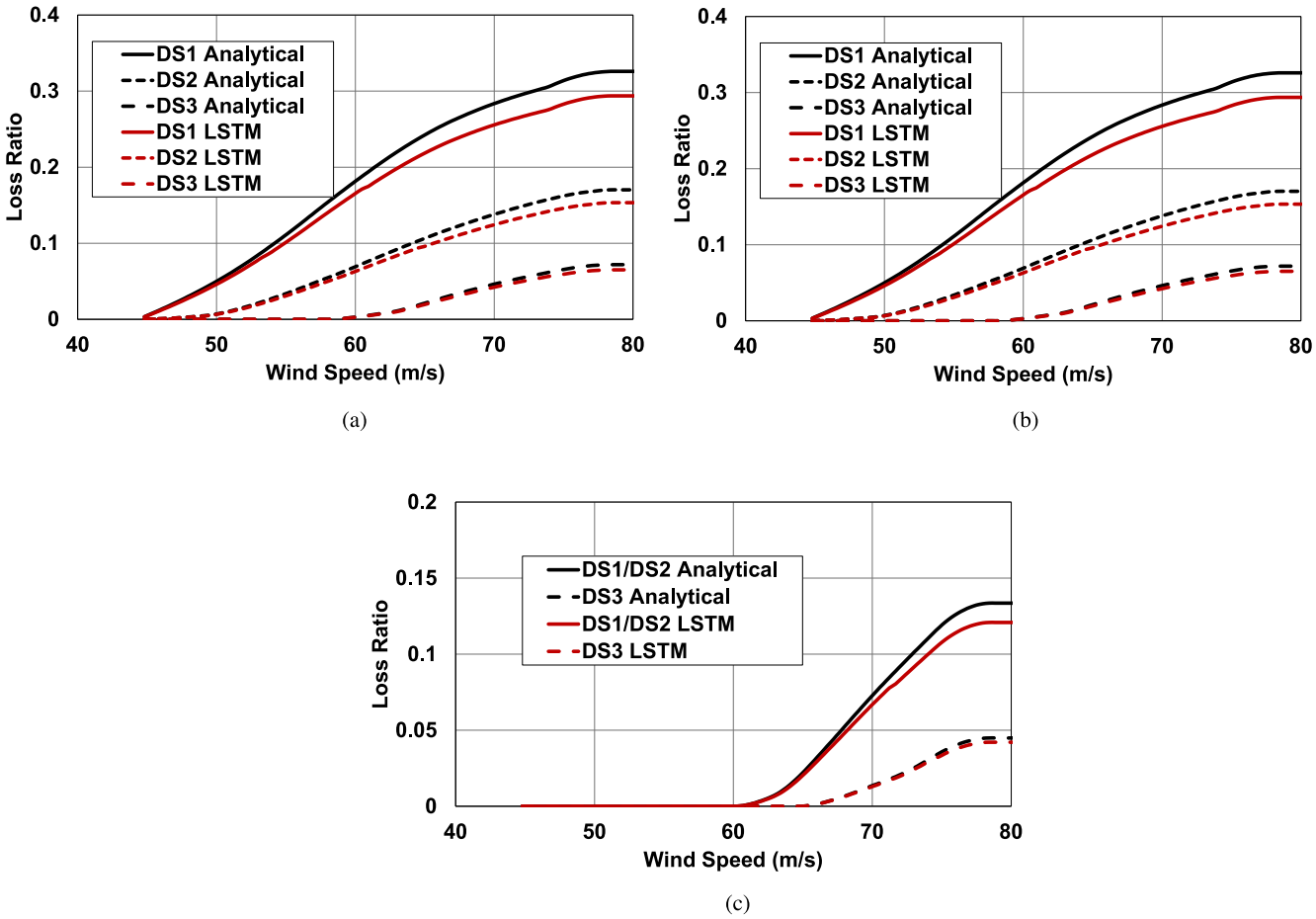

Fig. 15. Loss ratios of the chosen fragility groups (a) cold formed steel walls (b) gypsum partition walls and (c) welded column splice.

itself. The comparison of loss ratios for the fragility groups chosen in the study are given in Fig. 15. The predictions follow similar trends between LSTM and analytical models with the LSTM models slightly underpredicting the loss ratios than the analytical models. The improvement of results by changing the training to testing ratios or performing higher number of predictions within smaller intervals of wind speeds can be explored in future studies.

7. Conclusions

PBWE is identified as the preferred design methodology for tall buildings subject to wind actions. The wind actions on buildings are nearly continuous and could last between a few minutes to multiple hours. Dynamic time-history analysis of a tall building model under wind loads lasting for hours can be tedious aand requires high computaitonal power. To address these aspects, this research aimed to provide accurate structural responses by implementing data-driven techniques using limited numerical and experimental data. An LSTM model was developed to predict the nonlinear structural response of tall buildings under sustained wind loads for longer durations. The data-driven model was proposed as an alternative to the computationally expensive and time intensive finite element analyses. The model was expected to make accurate predictions of structural response and thus reduce the computational effort significantly in the response evaluation and damage quantification. The structural responses chosen were the story displacements and floor accelerations. The architecture of a single LSTM cell was explored and that of the complete LSTM model developed for the study was presented. The developed model was then tested to make predictions on a 44-story tall building using the nonlinear dynamic time-history analyses data from smaller datasets. The LSTM model was optimized for performance by choosing stack size and epoch numbers which resulted in the highest accuracy with minimum computational cost. The results obtained from the predictions were presented and showed reasonably accurate structural responses. True error was used as the metric for error quantification.

The LSTM model was then tested using the data from an experimental study on the aeroelastic model of the CAARC building configuration. The experimental studies were conducted at AABL WST Laboratory at Iowa State University. The LSTM model used a persistence forecast technique where the output from the previous time step was used to make predictions for the current time step. The predictions were found to be highly accurate and the model was also able to capture the maximum responses. The case studies also showed that LSTM was able to capture the maximum responses accurately with a very limited amount of training data. Lastly, the capability of LSTM to predict losses incurred under wind actions is tested and compared with that of analytical models.

CRediT authorship contribution statement

Smrithi Preetha Hareendran: Conceptualization, Methodology, Data curation, Software, Writing – original draft. **Alice Alipour:** Conceptualization, Methodology, Supervision, Funding acquisition, Validation, Writing – review & editing.

Declaration of competing interest

The authors have no conflict to declare.

Data availability

No data was used for the research described in the article.

Acknowledgments

This paper is based upon work supported by the National Science Foundation under Grant Nos. 1826356 and 1827774. Their support is gratefully acknowledged. Any opinions, findings, and conclusions or recommendations expressed in this material are those of the authors and do not necessarily reflect the views of the sponsor.

References

[1] M. Jafari, A. Alipour, Methodologies to mitigate wind-induced vibration of tall buildings: A state-of-the-art review, J. Build. Eng. 33 (2021) 101582, 1–25.
[2] M. Jafari, A. Alipour, Aerodynamic shape optimization of rectangular and elliptical double-skin façades to mitigate wind-induced effects on tall buildings, J. Wind Eng. Ind. Aerodyn. 213 (2021) 104586, 1–25.
[3] M. Jafari, A. Alipour, Review of approaches, opportunities, and future directions for improving aerodynamics of tall buildings with smart facades, J. Sustain. Cities Soc. 72 (2021) 102979, 1–20.
[4] K. Abdelaziz, A. Alipour, J. Hobeck, A smart façade system controller for optimized wind-induced vibration mitigation in tall buildings, J. Wind Eng. Ind. Aerodyn. 212 (2021) 104601, 1–10.
[5] J. Martin, A. Alipour, P. Sarkar, Fragility surfaces for multi-hazard analysis of suspension bridges under earthquakes and microbursts, Journal of Engineering Structures 197 (2019) 109169, pp. 1–13.
[6] L. Micheli, A. Alipour, S. Laflamme, P. Sarkar, Performance-based design with life-cycle cost assessment for damping systems integrated in wind excited tall buildings, J. Eng. Struct. 195 (2019) 438–451.
[7] L. Micheli, L. Cao, S. Laflamme, A. Alipour, Life cycle cost evaluation strategy for high performance control systems under uncertainties, ASCE J. Eng. Mech. 146 (2) (2020) 04019134, 1–15.
[8] L. Micheli, J. Hong, S. Laflamme, A. Alipour, Surrogate models for high performance control systems in wind-excited tall buildings, J. Appl. Soft Comput. 90 (2020) 106133, 1–15.
[9] L. Micheli, A. Alipour, S. Laflamme, Multiple-surrogate models for probabilistic performance assessment of wind-excited tall buildings under uncertainties, ASCE-ASME J. Risk Uncertain. Eng. Syst. A 6 (4) (2020) 04020042, 1–12.
[10] L. Micheli, A. Alipour, S. Laflamme, Life-cycle cost optimization of wind-excited tall buildings using surrogate models, J. Struct. Des. Tall Spec. Build. 30 (2021) E1840, 1–16.
[11] M. Ciampoli, F. Petrini, Performance-based aeolian risk assessment and reduction for tall buildings, Probab. Eng. Mech. (2012) 75–84, http://dx.doi.org/10.1016/j.probengmech.2011.08.013.
[12] M. Ciampoli, F. Petrini, G. Augusti, Performance-based wind engineering: Towards a general procedure, Struct. Saf. 33 (6) 367–378.
[13] F. Petrini, M. Ciampoli, Performance-based wind design of tall buildings, Struct. Infrastruct. Eng. 8 (2012) 954–966, http://dx.doi.org/10.1080/15732479.2011.574815.
[14] F. Petrini, K. Gkoumas, F. Bontempi, Damage and loss evaluation in the performance-based wind engineering, safety, reliability, risk and life-cycle performance of structures and infrastructures, in: Proceedings of the 11th International Conference on Structural Safety and Reliability, ICOSSAR 2013, 2013, pp. 1791–1797, http://dx.doi.org/10.1201/b16387-261.
[15] ASCE, Prestandard for Performance-Based Wind Design, 2019, http://dx.doi.org/10.1061/9780784482186.
[16] ASCE, ASCE 07-16 Minimum Design Loads on Buildings and Other Structures, 2016.
[17] J.S. Pei, A.W. Smyth, E.B. Kosmatopoulos, Analysis and modification of Volterra/Wiener neural networks for the adaptive identification of nonlinear hysteretic dynamic systems, J. Sound Vib. 275 (2004) 693–718, http://dx.doi.org/10.1016/j.jsv.2003.06.005.
[18] A.W. Smyth, J.S. Pei, S.F. Masri, System identification of the Vincent Thomas suspension bridge using earthquake records, Earthq. Eng. Struct. Dyn. 32 (2003) 339–367, http://dx.doi.org/10.1002/eqe.226.
[19] G.P. Zhang, B.E. Patuwo, M.Y. Hu, A simulation study of artificial neural networks for nonlinear time-series forecasting, Comput. Oper. Res. 28 (2001).
[20] B. Xu, Z. Wu, G. Chen, K. Yokoyama, Direct identification of structural parameters from dynamic responses with neural networks, Eng. Appl. Artif. Intell. 17 (2004) 931–943, http://dx.doi.org/10.1016/j.engappai.2004.08.010.
[21] Y. Wang, H. Li, W. Chong, R.Z. Ying, Artificial neural network prediction for seismic response of bridge structure, in: International Conference on Artificial Intelligence and Computational Intelligence, 2009.
[22] F. Karim, S. Majumdar, H. Darabi, S. Chen, LSTM fully convolutional networks for time series classification, IEEE Access 6 (2017) 1662–1669, http://dx.doi.org/10.1109/ACCESS.2017.2779939.
[23] D. Yinfeng, L. Yingmin, L. Ming, X. Mingkui, Nonlinear structural response prediction based on support vector machines, J. Sound Vib. 311 (2008) 886–897, http://dx.doi.org/10.1016/j.jsv.2007.09.054.
[24] T. Kim, O.S. Kwon, J. Song, Response prediction of nonlinear hysteretic systems by deep neural networks, Neural Netw. 111 (2019) 1–10, http://dx.doi.org/10.1016/j.neunet.2018.12.005.
[25] J.Y. Fu, S.G. Liang, Z.N. Xie, Prediction of wind loads on a large flat roof using fuzzy neural networks, Eng. Struct..
[26] J.Y. Fu, S.G. Liang, Q.S. Li, Prediction of wind-induced pressures on a large gymnasium roof using artificial neural networks, Comput. Struct. 85 (2007) 179–192, http://dx.doi.org/10.1016/j.compstruc.2006.08.070.
[27] Y.V. Arvind, Analysis of tall building for across wind response, Int. J. Civ. Struct. Eng. 2 (2012) http://dx.doi.org/10.6088/ijcser.00202030024.
[28] T.J. Nikose, R.S. Sonparote, Dynamic along wind response of tall buildings using Artificial Neural Network, Cluster Comput. 22 (2019) 3231–3246, http://dx.doi.org/10.1007/s10586-018-2027-0.
[29] T.J. Nikose, R.S. Sonparote, Computing dynamic across-wind response of tall buildings using artificial neural network, J. Supercomput. 76 (2020) 3788–3813, http://dx.doi.org/10.1007/s11227-018-2708-8.
[30] T.J. Nikose, R.S. Sonparote, Dynamic wind response of tall buildings using artificial neural network, Struct. Des. Tall Special Build. 28 (2019) http://dx.doi.org/10.1002/tal.1657.
[31] T.J. Nikose, R.S. Sonparote, Application of artificial neural network for predicting dynamic along-wind response of tall buildings, Struct. Des. Tall Special Build. 30 (2021) http://dx.doi.org/10.1002/tal.1837.
[32] H. Dongmei, H. Shiqing, H. Xuhui, Z. Xue, Prediction of wind loads on high-rise building using a BP neural network combined with POD, J. Wind Eng. Ind. Aerodyn. 170 (2017) 1–17, http://dx.doi.org/10.1016/j.jweia.2017.07.021.
[33] F. Bre, J.M. Gimenez, V.D. Fachinotti, Prediction of wind pressure coefficients on building surfaces using artificial neural networks, Energy Build. 158 (2018) 1429–1441, http://dx.doi.org/10.1016/j.enbuild.2017.11.045.
[34] J. Tian, K.R. Gurley, M.T. Diaz, P.L. Fernández-Cabán, F.J. Masters, R. Fang, Low-rise gable roof buildings pressure prediction using deep neural networks, J. Wind Eng. Ind. Aerodyn. 196 (2020) http://dx.doi.org/10.1016/j.jweia.2019.104026.
[35] N.D. Lagaros, M. Papadrakakis, Neural network based prediction schemes of the non-linear seismic response of 3D buildings, in: Advances in Engineering Software, Elsevier Ltd, 2012, pp. 92–115, http://dx.doi.org/10.1016/j.advengsoft.2011.05.033.
[36] R. Guarize, N.A.F. Matos, L.V.S. Sagrilo, E.C.P. Lima, Neural networks in the dynamic response analysis of slender marine structures, Appl. Ocean Res. 29 (2007) 191–198, http://dx.doi.org/10.1016/j.apor.2008.01.002.
[37] H. Wang, T. Wu, Knowledge-enhanced deep learning for wind-induced nonlinear structural dynamic analysis, J. Struct. Eng. 146 (2020) 04020235, http://dx.doi.org/10.1061/(asce)st.1943-541x.0002802.
[38] R. Zhang, Y. Liu, H. Sun, Physics-informed multi-LSTM networks for metamodeling of nonlinear structures, 2020, http://dx.doi.org/10.1016/j.cma.2020.113226.
[39] R. Zhang, Z. Chen, S. Chen, J. Zheng, O. Büyüköztürk, H. Sun, Deep long short-term memory networks for nonlinear structural seismic response prediction, Comput. Struct. 220 (2019) 55–68, http://dx.doi.org/10.1016/j.compstruc.2019.05.006.
[40] H. Peng, J. Yan, Y. Yu, Y. Luo, Time series estimation based on deep learning for structural dynamic nonlinear prediction, Structures 29 (2021) 1016–1031, http://dx.doi.org/10.1016/j.istruc.2020.11.049.
[41] F. Hou, P.P. Sarkar, Journal of Wind Engineering & Industrial Aerodynamics A time-domain method for predicting wind-induced buffeting response of tall buildings, J. Wind Eng. Ind. Aerodyn. 182 (2018) 61–71, http://dx.doi.org/10.1016/j.jweia.2018.09.013.
[42] S.P. Hareendran, A. Alipour, B. Shafei, P. Sarkar, Performance-based wind design of tall buildings considering the nonlinearity in building response, ASCE J. Struct. Eng. 148 (9) (2022).
[43] International Code Council, International Building Code, Falls Church, VA, 2018.
[44] American Institute of Steel Construction, Specification for Structural Steel Buildings (ANSI/AISC 360-16), Chicago, IL, 2016.
[45] ACI Committee, Building Code Requirements for Structural Concrete (ACI 318-19), Farmington Hills, MI, 2019.
[46] CSI, SAP2000-Integrated Software for Structural Analysis and Design.
[47] F. McKenna, M.H. Scott, G.L. Fenves, Nonlinear finite-element analysis software architecture using object composition, J. Comput. Civ. Eng. 24 (2010) 95–107.
[48] F. Hou, P.P. Sarkar, Time-domain model for prediction of generalized 3DOF buffeting response of tall buildings using 2D aerodynamic sectional properties, Eng. Struct. 232 (2021).